Chemical Physics Letters 485 (2010) 275–280

Contents lists available at ScienceDirect

Chemical Physics Letters

journal homepage: www.elsevier.com/locate/cplett

Proton micro-magic-angle-spinning NMR spectroscopy of nanoliter samples

Andreas Brinkmann [a,b,*], Suresh Kumar Vasa [a], Hans Janssen [a], Arno P.M. Kentgens [a,*]

[a] Physical Chemistry/Solid State NMR, Institute for Molecules and Materials, Radboud University Nijmegen, P.O. Box 9010, 6500 GL Nijmegen, The Netherlands
[b] Steacie Institute for Molecular Sciences, National Research Council, 1200 Montreal Road, M-40 Ottawa, Ontario, Canada K1A 0R6

ARTICLE INFO

Article history:
Received 22 October 2009
In final form 16 December 2009
Available online 23 December 2009

ABSTRACT

We present our recent progress in the development of micro-magic-angle-spinning solenoid-based probeheads for the application in high-resolution ^{1}H solid-state NMR of nanoliter sample volumes. The use of fused-silica capillaries as sample holders results in spectra without any ^{1}H background signal. It is possible to obtain ^{1}H spectra of 40–80 nl samples in a few scans. We obtained high-resolution ^{1}H spectra employing different homonuclear decoupling sequences on powdered samples of L-alanine, the tripeptide AGG, and a single crystal of L-tyrosine·HCl. In addition, we recorded high-resolution two-dimensional proton-detected ^{1}H–^{13}C heteronuclear correlation spectra of [U-$^{13}C_3$,^{15}N]-L-alanine and AGG with natural abundant isotope distribution.

1. Introduction

Solid-state NMR spectroscopy is a powerful method to obtain detailed structural information in systems that do not posses long-range order, ranging from disordered inorganic, organic and hybrid materials to biological macromolecules [1]. In order to achieve NMR spectra with high resolution and sensitivity, most of these applications require magic-angle spinning (MAS), where the sample is rapidly rotated about an axis at the *magic angle* ($\approx 54.74^{\circ}$) with respect to the static magnetic field, which attenuates the effect of anisotropic spin interactions. However, many materials studied by solid-state NMR are on the one hand only available in limited amounts such as rare minerals, biological and newly developed functional materials. On the other hand the total sample volume may be limited by the specific geometry of the sample in question, e.g. in case single crystals, fibers or thin films need to be analyzed. In order to maximize the sensitivity of solid-state NMR experiments under these circumstances the use of microcoils (diameters below 1 mm) for excitation and detection is favorable. Two approaches have been presented recently to combine solenoid microcoils and MAS: Firstly, the nanoliter sample container is 'piggy-backed' onto a regular size solid-state NMR rotor and spun inside the microcoil, which is mounted on top of the regular MAS stator [2,3]. Secondly, the microcoil is loaded into a regular MAS rotor and inductively coupled to the regular macroscopic NMR detection coil [4]. Both approaches have so far been used to obtain ^{1}H spectra [4], ^{13}C cross-polarization (CP) MAS spectra [2,3], ^{13}C double-quantum spectra [3], and ^{29}Si one-dimensional (1D) spectra [4]. In addition, ^{27}Al 1D MAS spectra were recorded on a single crystal of mesolite [3]. Inukai and Takeda showed that the high rf field strengths available in microcoils lead to higher efficiencies in the excitation of multiple-quantum (MQ) coherences in half-integer quadrupolar nuclei [5]. Furthermore, Vasa et al. determined the orientation of the ^{23}Na quadrupolar tensor in $NaNO_3$ using rotor-synchronized MAS [6] in a single crystal of 35 nl volume [7].

Considering the small sample volumes available in micro-magic-angle-spinning (microMAS) NMR studies it is attractive to focus on abundant and highly-sensitive nuclei. Therefore the possibility to obtain high-resolution ^{1}H NMR spectra is of particular interest in the context of micoMAS. In recent years the availability of high external magnetic fields combined with the development of ultra-fast MAS probeheads and improved radiofrequency (rf) pulse sequences for homonuclear decoupling has lead to an increasing application of ^{1}H MAS NMR spectroscopy in material science [8,9]. Although ultrafast MAS leads to considerably improved proton resolution by attenuating the influence of the strong ^{1}H–^{1}H couplings, better results can so far still be achieved by combining MAS with applying homonuclear dipolar decoupling sequences to enhance the averaging of the ^{1}H homonuclear dipolar couplings [8,9]. The homonuclear decoupling sequences Frequency-Switched Lee-Goldburg (FSLG) [10–12] and its close relative Phase-Modulated Lee-Goldburg (PMLG) [13–15] are based on theoretical arguments by average Hamiltonian [16] and Floquet theory [17] to suppress the homonuclear dipolar ^{1}H–^{1}H couplings and their commutators with other spin interactions to a certain order. The DUMBO ('decoupling using mind-boggling optimization') sequence has been developed by numerical optimization using a two-spin system [18,19]. A more powerful approach is the direct optimization of this type of sequence on the NMR spectrometer

* Corresponding authors. Address: Steacie Institute for Molecular Sciences, National Research Council, 1200 Montreal Road, M-40 Ottawa, Ontario, Canada K1A 0R6 (A. Brinkmann). Fax: +1 613 990 1555 (A. Brinkmann).
E-mail addresses: Andreas.Brinkmann@nrc-cnrc.gc.ca (A. Brinkmann), A.Kentgens@science.ru.nl (A.P.M. Kentgens).

0009-2614/$ - see front matter Crown Copyright © 2009 Published by Elsevier B.V. All rights reserved.
doi:10.1016/j.cplett.2009.12.054

that has led to the eDUMBO sequence, since imperfections in the experimental setup are inherently included in the optimization [20]. These experimental imperfections include the finite speed and glitches during switching of the rf phases and amplitudes, rf inhomogeneities and rf phase transients. All the homonuclear decoupling sequence mentioned so far cause transverse ^{1}H magnetization to evolve in a plane perpendicular to an effective field that is tilted at the magic-angle with respect to the z-axis in the rotating frame. In order to avoid artifacts in the resulting high-resolution ^{1}H spectra, this usually requires careful optimization of the ^{1}H excitation pulses that rotate the longitudinal magnetization into the evolution plane. Recently, supercycled versions of PMLG and DUMBO have been presented that perform an effective z-rotation of the ^{1}H transverse magnetization resulting in artifact-free ^{1}H spectra [21,22]. Furthermore, it has been shown that both PMLG and DUMBO/eDUMBO can be successfully applied under ultrafast MAS conditions [21,23,24], although this does not lead to improved resolution compared to using moderate spinning frequencies. Other factors such as the size of the external magnetic field, rf inhomogeneity and phase transients appear to be significantly more important.

If windows are incorporated in these homonuclear decoupling pulse sequences, it becomes possible to apply them during direct detection of the ^{1}H NMR signal, where the datapoints are recorded during the pulse sequence windows [12,25,19]. This is especially attractive since it allows to *indirectly* or *inversely* detect the NMR signal of a low-abundant and less-sensitive spin species via ^{1}H. Ishii and Tycko have shown that this is especially favorable for nuclei with low gyromagnetic ratio γ if the ^{1}H NMR lines are narrow and efficient polarization transfer is possible [26]. Inverse detection of ^{15}N signals at fast MAS to achieve ^{1}H resolution has been used by Spiess and coworkers to study multiple hydrogen-bonded systems [27–29]. Furthermore, the group of Pruski designed both ^{1}H detected two-dimensional (2D) ^{1}H–^{13}C through-space and through-bond experiments at fast MAS and applied them to organic–inorganic hybrid materials [30,31]. In addition, Rienstra and coworkers used both ^{1}H detected ^{1}H–^{13}C and ^{1}H–^{15}N 2D heteronuclear correlation (HETCOR) spectroscopy to analyze pharmaceutical compounds and biological macromolecules [32–34].

In this letter we describe the use of proton-free fused-silica capillaries with outer diameters of 400 μm as sample holders for the application in high-resolution ^{1}H solid-state microMAS NMR of nanoliter samples employing different homonuclear decoupling sequences.

2. Experimental methods

2.1. MicroMAS probehead for ^{1}H spectroscopy

The microMAS probehead used in this work is designed following the same principles described in Ref. [2]: a solenoid microcoil is integrated into a double-sided circuit board that is mounted on a regular 2.5 mm Varian MAS pencil stator as shown in Fig. 1c. The rf coil is made from isolated copper wire with a diameter of 115 μm that is wound into 7.5 turns with the help of a glass matrix. The resulting solenoid coil has inner and outer diameters of 450 and 680 μm, respectively. The double-tunable rf circuit of the microcoil provides a ^{1}H channel tuneable at 400 MHz with $Q_H = 45$ and an X channel with $Q_X = 24$ at 100.58 MHz resonance frequency.

In order to ensure the complete absence of ^{1}H background signal, capillaries from fused silica with inner and outer diameters of 320 and 400 μm, respectively, are used as sample holders. The capillary is inserted into a Kel-F holder that can be fitted tightly into a 2.5 mm Varian rotor, replacing its usual Vespel end-cap. Before filling the sample into the capillary, a Kel-F spacer is inserted. Typical sample heights of 800–1100 μm leave some space at the top of the capillary to close it off with Teflon tape. As a result sample volumes are in the order of 64–88 nl. Fig. 1a shows a picture of a filled capillary inside the Kel-F holder, which is pushed into the 2.5 mm rotor using a dedicated custom-made tool shown in Fig. 1b.

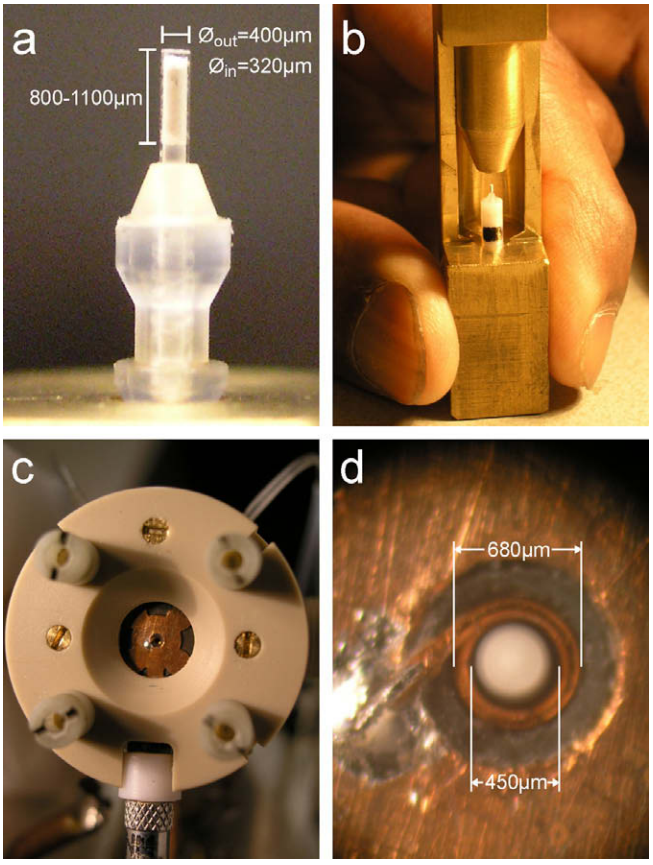

Fig. 1. (a) Kel-F holder with inserted fused-silica capillary containing powdered sample material. The capillary has inner and outer diameters of 320 and 400 μm, respectively. The sample height is 800–1100 μm leaving some space to close off the capillary with Teflon tape. As a result typical sample volumes are in the order of 64–88 nl. (b) 2.5 mm Varian rotor with Kel-F holder and capillary inside the custom-made press-on tool. (c) Upper front of the 2.5 mm Varian stator with the mounted holder of the solenoid microcoil. (d) Microscope image of the silica capillary spinning inside the microcoil. The rf coil possesses 7.5 windings, where the isolated copper wire has a diameter of 115 μm. The inner and outer diameters of the rf coil are 450 and 680 μm, respectively.

The 2.5 mm Varian MAS stator is modified to allow loading of the rotor from the bottom of the stator. The height of the rotor is adjusted so that the sample volume sits inside the microcoil and stable spinning of the rotor is accomplished, which we could easily achieve for spinning frequencies up to 20 kHz. The MAS stator is fitted with a separate circuit tuned for ^{23}Na observation, which allows to adjust the angle of the spinning axis with respect to the external magnetic field to the magic-angle using $NaNO_3$ that occupies the regular sample volume of the 2.5 mm macro-rotor. It should be noted that this opens the possibility for parallelizing micro and macro experiments.

The nanoliter sample inside the fused-silica capillary lies outside the center of the regular shim coils, making it difficult to shim the external field at the exact nanoliter sample position. However, we achieved a full width at half maximum (FWHM) of 19 Hz for the ^{1}H resonance in a sample of silicon rubber. (In a future setup additional small Helmholtz coils will allow to shim the external magnetic field along the direction of the spinner axis at the location of the nanoliter sample volume.)

Table 1
Rf field strengths ω_1 as a function of the rf power P for the X channel at $^{13}C/^{23}Na$ reference frequency and for the ^1H channel at 400 MHz reference frequency.

$P(^{13}C/^{23}Na)$ (W)	$\omega_1/2\pi(^{13}C/^{23}Na)$ (kHz)	$P(^1H)$ (W)	$\omega_1/2\pi(^1H)$ (kHz)
0.6	46	0.6	128
83	556	2.5	355
920	1670	10.5	786

Table 1 shows the rf field strength that can be achieved on the X and ^1H channels as a function of the rf input powers used in each case. It shows that the efficiency $B_1/\sqrt{P}$ (where B_1 is the rf field generated in the coil by the rf power P) for the micro rf circuit is about 13 times better than that of the 2.5 mm MAS rf circuit for the proton channel and 4.7 times better for the X-channel. An advantage of ^1H detection using microMAS at high external magnetic fields is that the coil sizes are still small with respect to the rf wavelength and therefore are hardly affected by wave compression, which negatively influences the performance of larger coils at high rf frequencies [35].

2.2. Solid-state NMR experiments

All experiments were done on a Varian NMR System (VNMRS) at an external field of 9.4 T (400 MHz proton frequency). Fig. 2 shows the different pulse sequences used to obtain the high-resolution ^1H spectra and ^{13}C–^1H HETCOR spectra presented in this work by employing homonuclear decoupling sequences to suppress the strong ^1H–^1H dipolar couplings at moderare to fast sample spinning frequencies. The pulse scheme in Fig. 2a allows to record a 2D ^1H spectrum, where the indirect dimension represents the high-resolution, homonuclear decoupled ^1H dimension and the direct dimension corresponds to the low-resolution ^1H dimension. The first 90° pulse generates transverse ^1H magnetization that evolves perpendicular to the effective field of the homonuclear decoupling sequence applied during the evolution interval t_1. We used both FSLG [10–12] and eDUMBO [20] windowless homonuclear decoupling, whose effective fields enclose an angle of θ close to the magic-angle of 54.74° with respect to the z-axis in the rotating frame. Therefore, the following θ pulse rotates the magnetization into the xy-plane. A pair of 90° pulses allows to select longitudinal magnetization by an appropriate phase cycle before the ^1H NMR signal is detected during the time interval t_2.

Fig. 2b shows the pulse sequence used to obtain 1D high-resolution ^1H spectra by employing the windowed homonuclear decoupling sequence wDUMBO [19], where the datapoints of the ^1H signal are recorded during the pulse sequence windows. The rf phase of the excitation pulses with flip-angles 90° and θ were adjusted as described in Ref. [19] to minimize the artifacts in the frequency domain at the center of the spectral window.

Finally, the pulse scheme in Fig. 2c was used to record indirectly/inversely-(^1H)-detected 2D ^1H–^{13}C HETCOR spectra. It is applicable for the spectral correlation of any heteronuclei and ^1H in general. First the heteronuclear S-spin magnetization is enhanced by adiabatic cross-polarization [36] and stored along the z-axis in the rotating frame for a time-interval τ_f, during which the remaining direct transverse ^1H magnetization is allowed to dephase. Subsequently, after evolution during t_1, the transverse S-spin magnetization is transferred to the ^1H-spins by ramped Lee-Goldburg cross-polarization [37–39]. The resulting ^1H magnetization is aligned along the z-axis in the rotating frame by a θ_1 pulse and detected by a wDUMBO sequence as in Fig. 2b. High-rf-field ^1H decoupling using the XiX scheme [40,41] is applied during t_1, and optionally low-rf-field S-spin continuous-wave decoupling is used during detection of the ^1H signal.

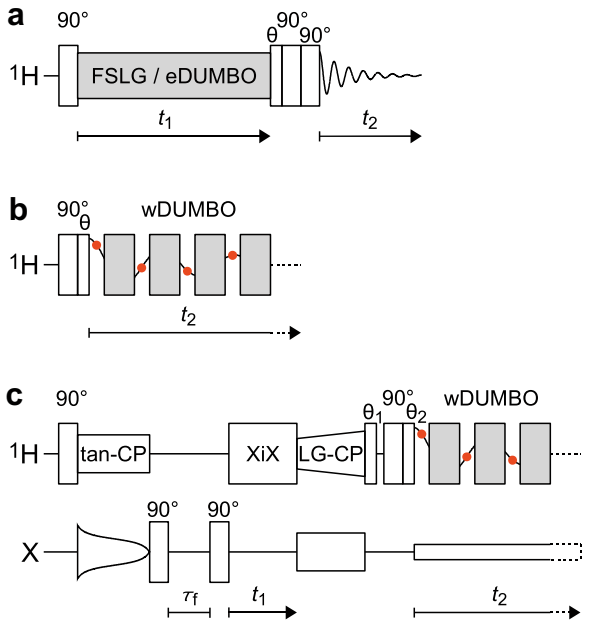

Fig. 2. (a) Rf pulse sequence to obtain 2D ^1H spectra, where homonuclear decoupling during t_1 by either FSLG or eDUMBO leads to the high-resolution indirect dimension in the resulting 2D spectrum. θ indicates an rf pulse with the flip-angle close to 54.74°. (b) Rf pulse sequence to obtain high-resolution ^1H spectra in the direct dimesion by applying a windowed version of a homonuclear decoupling sequence (here wDUMBO), where datapoints are collected during the sequence windows. (c) Rf pulse sequence to obtain 2D HETCOR spectra between ^1H and the less sensitive spin species S, whose spectrum is *indirectly detected* via the ^1H, which are observed directly during a wDUMBO sequence.

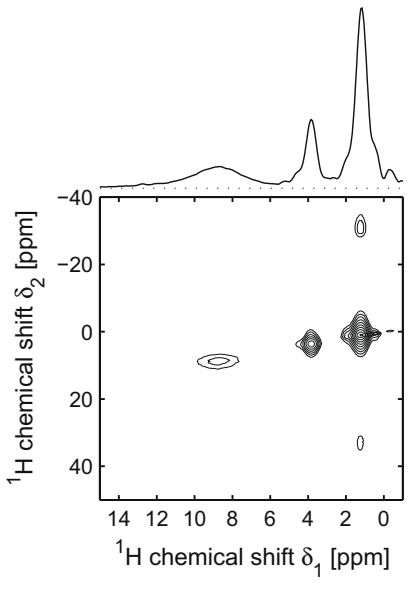

Fig. 3. Experimental 2D ^1H spectrum of about 80 nl L-alanine powder obtained at an external field of 9.4 T and a spinning frequency of 12 kHz, where windowless eDUMBO homonuclear decoupling with an rf nutation frequency of 82 kHz, a DUMBO cycle time of 36.8 μs and an overall rf offset of −1 kHz was applied in the indirect high-resolution ^1H dimension. The interval t_1 was incremented in steps of one DUMBO cycle, where 8 transients were added up for each increment and the delay between experiments was 4 s. A total of 178 t_1 increments were collected following the States procedure. The skyline projection onto the indirect δ_1 dimension is shown on the top. The unscaled ^1H linewidths (FWHM) for the different resonances are $\Delta(CH) = 159$ Hz, $\Delta(CH_3) = 166$ Hz and $\Delta(NH_3^+) = 698$ Hz.

Under the DUMBO and FSLG homonuclear decoupling sequences the isotropic chemical shifts of the protons are scaled by a factor that we determined experimentally through acquiring a series of two-dimensional ^{1}H spectra with different offsets for the rf carrier frequency. The experimentally determined values for the scaling factors were used to correct the scaling of the ^{1}H chemical shift dimension.

3. Results and discussion

In a first step, we evaluated the performance of the microMAS setup to obtain high-resolution ^{1}H spectra by applying windowless homonuclear decoupling sequences of type eDUMBO and FSLG. These experiments were done at a spinning frequency of 12 kHz using the pulse sequence shown in Fig. 2a. The resulting 2D ^{1}H spectrum of a sample of about 80 nl of powdered L-alanine using eDUMBO homonuclear decoupling is presented in Fig. 3. The nutation frequency of the ^{1}H rf field during the eDUMBO sequence was 82 kHz, which was achieved by a few hundred mW of ^{1}H power. Hence, conventional rf nutation frequencies can easily achieved with very low powers, requiring only small amplification of the rf transmitter output.

We determined the unscaled linewidths as the full width at half maximum (FWHM) of the different resonances in the high-resolution ^{1}H dimension to be 698 Hz (1.75 ppm), 159 Hz (0.40 ppm) and 166 Hz (0.41 ppm) for the NH_3^+, CH and CH_3 proton resonances, respectively. These values are in very good agreement to the linewidths achieved by Lesage et al. at 11.75 T external field using a conventional 4 mm CP MAS probe, where the sample volume was restricted to about 25 µl in the center of the rotor [19]. Hence, the rf homogeneity of the solenoid microcoil in our experimental setup is well suited for performing homonuclear decoupling. This is supported by the ^{1}H nutation spectrum obtained on a single crystal of L-tyrosine·HCl with the dimensions $230 \times 230 \times 800\ \mu m^3 \approx 42$ nl shown in Fig. 4. The rf inhomogeneity determined from this spectrum is 3%, which lets us conservatively specify the rf inhomogeneity for a completely filled sample volume inside the capillary to about 5%.

For the single-crystal of L-tyrosine·HCl we achieved better resolved ^{1}H spectra using FSLG homonuclear decoupling compared to using eDUMBO. The corresponding result is shown in Fig. 5, where the nutation frequency of the ^{1}H rf field during the FSLG sequence was 82 kHz. Comparing our result with recent results by Leskes et al. [21] obtained at 14.1 T, 65 kHz MAS frequency, employing wPMLG5$^{xx}_{mm}$ homonuclear decoupling, we could achieve comparable resolution. This proves that even at moderate MAS frequencies it is already possible to obtain the highest resolution in ^{1}H spectra using homonuclear decoupling based on DUMBO, FSLG or PMLG sequences. These results hold great promise for ^{1}H microMAS NMR experiments of mass-limited samples, especially if the high-resolution ^{1}H spectra are obtained by directly detecting the proton signals employing windowed versions of these homonuclear decoupling sequences, since already a single transient provides a sufficient signal-to-noise (S/N) ratio even for these limited sample quantities in the 40–80 nl sample volume regime. Improving the resolution of the ^{1}H spectra further by increasing the nutation frequency of rf fields during homonuclear decoupling was not successful at this stage, which we attribute to rf phase transients that scale with the size of the rf field.

A second step was to investigate the potential of inversely/indirectly detecting the spectra of potentially low abundant heteronuclei in nanoliter samples via the protons by detecting them using windowed homonuclear decoupling sequences. Therefore we recorded 2D ^{1}H-detected ^{1}H–^{13}C HETCOR spectra of [U-$^{13}C_3$, ^{15}N]-L-alanine and the tripeptide AGG (natural abundance distribution of isotopes) at 18 kHz spinning frequency. In both cases about 80 nl of sample was used and wDUMBO windowed homonuclear decoupling was applied during ^{1}H signal detection.

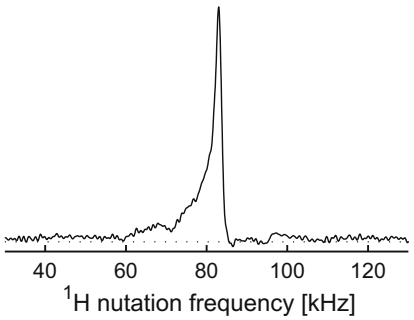

Fig. 4. Slice parallel to the indirect dimension through the maximum in the 2D ^{1}H nutation spectrum of a single crystal of L-tyrosine·HCl with the dimensions $230 \times 230 \times 800\ \mu m^3 \approx 42$ nl. The nutation spectrum was obtained at 9.4 T and 12 kHz MAS frequency by incrementing the duration of the ^{1}H excitation pulse in steps of 2 µs until a total of 1024 increments had been recorded. The ^{1}H nutation frequency results to 83.0 kHz with a FWHM of 2.2 kHz, corresponding to an rf inhomogeneity of 3%.

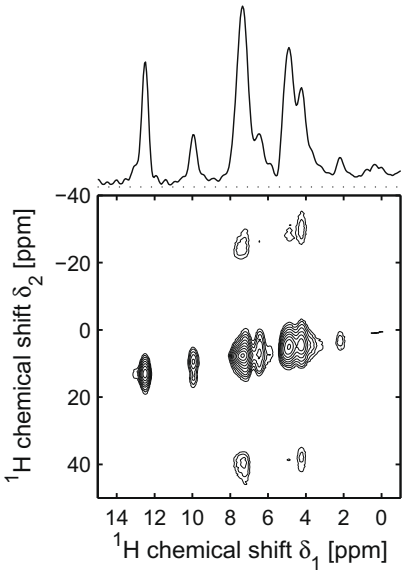

Fig. 5. Experimental 2D ^{1}H spectrum of a single crystal of L-tyrosine·HCl with the dimensions $230 \times 230 \times 800\ \mu m^3 \approx 42$ nl obtained at 9.4 T and 12 kHz MAS frequency, where FSLG homonuclear decoupling with an rf nutation frequency of 82 kHz, frequency jumps of ±57 735 and an overall rf offset of 2 kHz was applied in the indirect ^{1}H dimension. The frequency jumps were performed with a simultaneous 180° phase shift every 10 µs. The interval t_1 was incremented in steps of 40 µs, where 8 transients were added up for each increment and the delay between experiments was 4 s. A total of 237 increments were collected following the States procedure. The skyline projection onto the indirect δ_1 dimension is shown on the top.

The results obtained for [U-$^{13}C_3$, ^{15}N]-L-alanine are shown in Fig. 6, where (a) shows the directly-detected ^{1}H spectrum using wDUMBO and (b) shows the ^{1}H-detected 2D ^{1}H–^{13}C HETCOR spectrum. The HETCOR spectrum shows clearly the strong cross-peaks between the ^{13}C and ^{1}H sites in the CH and CH_3 groups. Because of the relatively long mixing interval of 1167 µs for the LG-CP, also crosspeaks of type (^{13}CH, C$^1H_3$) and ($^{13}CH_3$, C^{1}H) are visible. In addition, a small (^{13}CO, C$^1H_3$) cross-peak can be seen. The complete 2D spectrum was recorded in 13.5 h performing 186 t_1 increments with 32 transients each using the States procedure. This

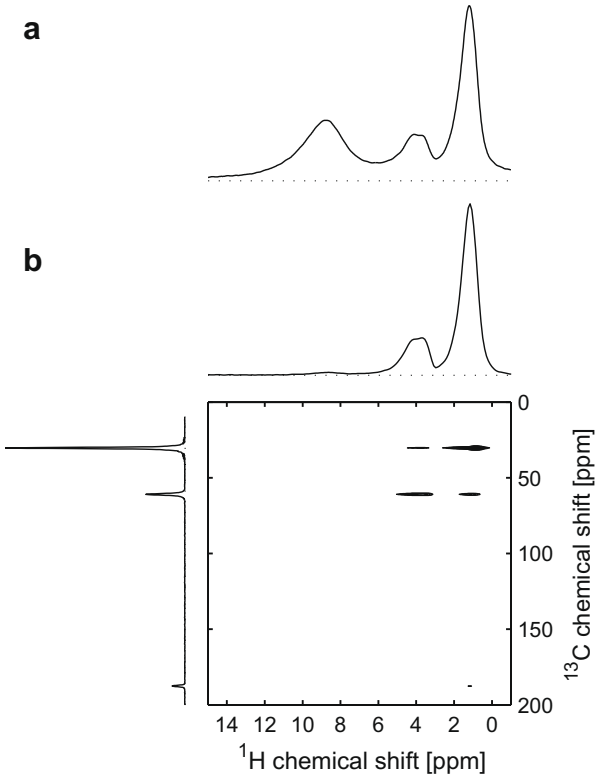

Fig. 6. (a) Directly detected ^{1}H spectrum of [U-$^{13}C_3$, ^{15}N]-L-alanine, recorded by adding 64 transients at 9.4 T and 18 kHz MAS frequency using the pulse sequence in Fig. 2b employing wDUMBO homonuclear decoupling with an rf nutation frequency of 156 kHz, a cycle time of 19.2 μs and an overall rf offset of 3.2 kHz. (b) Experimental ^{1}H-detected 2D ^{1}H–^{13}C HETCOR spectrum of [U-$^{13}C_3$, ^{15}N]-L-alanine obtained at the same experimental conditions as (a) using the pulse sequence shown in Fig. 2c. The intervals for tan- and LG-CP were 778 and 1167 μs, respectively. The ^{1}H rf offset during LG-CP was 68.772 kHz. XiX ^{1}H-decoupling with a nutation frequency of 230 kHz and a pulse duration of 157 μs was applied during the t_1 interval, and continuous-wave ^{13}C-decoupling with a nutation frequency of about 10 kHz was used during acquisition of the ^{1}H signal. The time interval for dephasing of direct ^{1}H magnetization was set to $\tau_f = 222$ μs. The interval t_1 was incremented in steps of 50 μs, where 32 transients were added up for each increment and the delay between experiments was 4 s. A total of 186 increments were collected following the States procedure, leading to a total experimental time of about 13.5 h. Skyline projections onto the ^{1}H and ^{13}C dimensions are shown on the top and left side of the 2D spectrum, respectively.

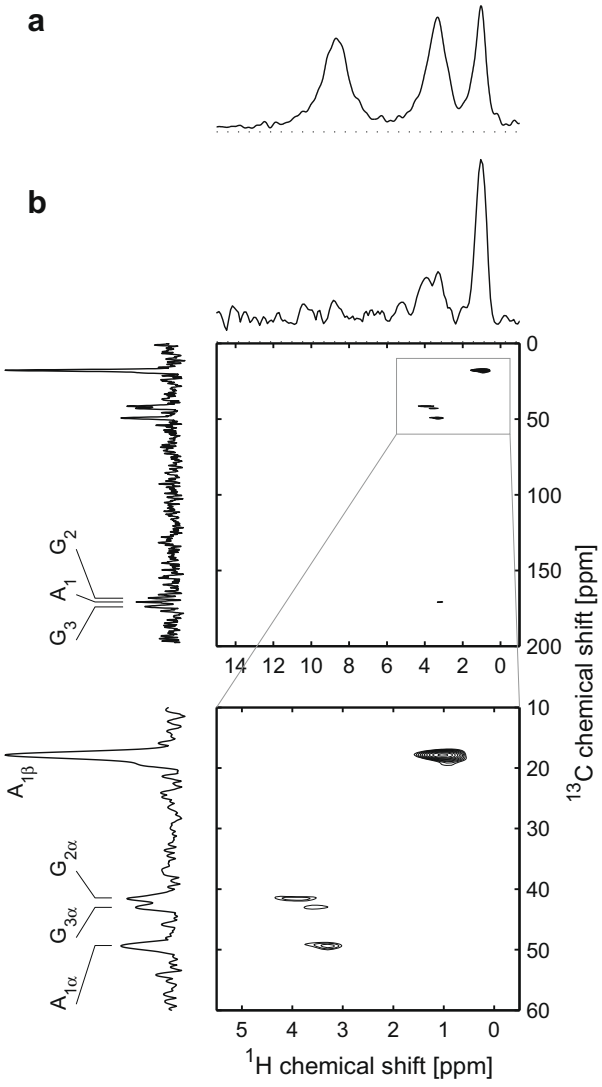

Fig. 7. (a) Directly detected ^{1}H spectrum of AGG, obtained by adding 8 transients at an external field of 9.4 T and a spinning frequency of 18 kHz using the pulse sequence in Fig. 2b employing wDUMBO with an rf nutation frequency of 153 kHz, a cycle time of 19.6 μs and an overall rf offset of 3.2 kHz. (b) Experimental ^{1}H-detected 2D ^{1}H–^{13}C HETCOR spectrum of AGG recorded at the same experimental conditions as (a) using the pulse sequence shown in Fig. 2c. The intervals for tan- and LG-CP were 778 and 500 μs, respectively. The ^{1}H rf offset during LG-CP was 72.42 kHz. XiX ^{1}H-decoupling with a nutation frequency of 200 kHz and a pulse duration of 158.3 μs was applied during the t_1 interval, and continuous-wave ^{13}C-decoupling with a nutation frequency of about 10 kHz was used during acquisition of the ^{1}H signal. The time interval for dephasing of direct ^{1}H magnetization was set to $\tau_f = 1$ ms. The interval t_1 was incremented in steps of 50 μs, where 608 transients were added up for each increment and the delay between experiments was 1.5 s. A total of 128 increments were collected following the States procedure, leading to a total experimental time of about 65 h. Skyline projections onto the ^{1}H and ^{13}C dimensions are shown on the top and left side of the 2D spectrum, respectively, where the assignment of the different ^{13}C resonances correct the one shown in Ref. [45].

clearly demonstrates the good feasibility of these type of experiments on isotopically labelled samples.

The results for the more challenging case of natural-abundance AGG are shown in Fig. 7, where the directly detected homonuclear decoupled ^{1}H spectrum is shown in (a) and the 2D ^{1}H-detected 2D ^{1}H–^{13}C HETCOR spectrum is presented in (b). In addition to the overview 2D HETCOR spectrum the enlarged part of the spectrum is shown where the correlation peaks of the different ^{13}C and ^{1}H sites of the CH, CH_2 and CH_3 groups can be found. The different cross-peaks are well-resolved and allow the assignment of the different isotropic chemical shifts, which is indicated in Fig. 7b for the different ^{13}C sites. We confirmed our assignment by density functional theory (DFT) calculations using QUANTUM ESPRESSO [42] explicitly taking the periodicity in the crystal structure of AGG [43] into account. Our assignment of the ^{13}C resonances is in agreement with the one of Luca et al. [44] and corrects the one presented recently in Ref. [45]. Interestingly, we found that the positions of some ^{13}C resonances measured using microMAS are significantly shifted compared to those measured using MAS in a conventional 3.2 mm rotor. Differences in chemical shifts by more than 1 ppm were observed for the $G_{2\alpha}$ (−2.4 ppm) aliphatic, and the G_2 (−1.2 ppm) and G_3 (−3.0 ppm) carboxyl carbon sites. We have no explanation for these changes in the chemical shift at this point. However, we suspect that differences in hydration and sample-heating during the macro- and microMAS experiments might be the cause for these differences. We are currently investigating these effects further.

The complete 2D ^{1}H–^{13}C HETCOR spectrum shown in Fig. 7b was obtained in 65 h by carrying out 128 t_1 increments each consisting of 608 transients obeying the States procedure. As a result

even ^{1}H–^{13}C HETCOR spectroscopy of nanoliter samples that are not isotopically enriched is feasible. However, our results also indicate that ^{1}H–^{15}N HETCOR spectroscopy realistically would require some isotopic enrichment in ^{15}N.

4. Conclusions and outlook

In this contribution, we presented a microMAS setup for high-resolution ^{1}H solid-state NMR spectroscopy using fused-silica capillaries as sample containers with about 64–88 nl sample volume. The 'piggy-back' setup on top of regular 2.5 mm MAS rotors allows for stable sample spinning up to 20 kHz. ^{1}H rf fields with nutation frequencies up to 800 kHz can be achieved by using 10 W of ^{1}H power, hence allowing the use of cost-efficient low-power rf amplifiers. In addition, we showed that the chosen solenoid microcoil setup is well suited to obtain high-resolution ^{1}H spectra by employing homonuclear decoupling sequences of types FSLG and eDUMBO. We found, however, that the optimal ^{1}H spectral resolution is achieved when using conventional ^{1}H rf field strengths in the order of 80–160 kHz, whereas higher rf field strengths degrade the spectral resolution. We attribute this effect to rf phase transient stemming from the resonant circuit of the microcoil. These transients increase in importance as their amplitude scales with the rf field [46] and because the effective pulses during the homonuclear decoupling sequences get shorter at higher rf fields. Hence, in order to profit from the high rf fields available in the microMAS setup, the development of improved homonuclear decoupling sequences is needed that are better compensated for these transients. Investigations in this direction following the eDUMBO principle of direct spectral optimization on the NMR spectrometer [20] are on the way in our laboratories. Furthermore, we demonstrated ^{1}H-detected 2D ^{1}H-^{13}C HETCOR spectroscopy both on isotopically enriched and natural abundance nanoliter samples using windowed homonuclear decoupling sequences during ^{1}H detection. This approach can easily be extended to ^{1}H-detected ^{15}N NMR of isotopically enriched samples using an appropriate double-tune microcoil circuit. The high rf fields strengths achievable would also be very beneficial for ^{1}H detected NMR spectroscopy of insensitive quadrupolar nuclei such as ^{14}N and ^{17}O [47,48]. The 'piggy-back' design can straightforwardly be extended to MAS rotors with smaller diameters, extending the use of microMAS into the ultra-fast spinning regime that would increase the resolution for directly detected ^{1}H spectra and the sensitivity for indirectly detected heteronuclei.

Acknowledgments

The authors thank Jan van Os and Gerrit Janssen for experimental help, Ernst van Eck for discussions and Peter Pallister for the help with QUANTUM ESPRESSO. We are grateful to Dave Rice and Vadim Zorin from Varian Inc. for their support. The Netherlands Organization for Scientific Research (NWO) is acknowledged for their financial support of the solid-state NMR facility for advanced material science and for sponsoring this research through an NWO-TOP grant.

References

[1] C.P. Grey, R. Tycko, Phys. Today 62 (2009) 44.
[2] J.W.G. Janssen, A. Brinkmann, E.R.H. van Eck, P.J.M. van Bentum, A.P.M. Kentgens, J. Am. Chem. Soc. 128 (2006) 8722.
[3] A.P.M. Kentgens et al., J. Chem. Phys. 128 (2008) 052202.
[4] D. Sakellariou, G. Le Goff, J.-F. Jacquinot, Nature 447 (2007) 694.
[5] M. Inukai, K. Takeda, Concepts Magn. Reson. B 33 (2008) 115.
[6] G.S. Harbison, V.-D. Vogt, H.W. Spiess, J. Chem. Phys. 86 (1987) 1206.
[7] S.K. Vasa, E. van Eck, H. Janssen, A. Kentgens, Full quadrupolar tensor determination by NMR using a micro-crystal spinning at the magic-angle, submitted for publication.
[8] S.P. Brown, Prog. NMR Spectrosc. 50 (2007) 199.
[9] S.P. Brown, Macromol. Rapid Commun. 30 (2009) 688.
[10] M. Mehring, J.S. Waugh, Phys. Rev. B 5 (1972) 3459.
[11] A. Bielecki, A.C. Kolbert, M.H. Levitt, Chem. Phys. Lett. 155 (1989) 341.
[12] M.H. Levitt, A.C. Kolbert, A. Bielecki, D.J. Ruben, Solid State NMR 2 (1993) 151.
[13] J. Ashida, D. Rice, Magn. Moments 8 (1996) 19 (a Varian publication).
[14] B.M. Fung, K. Ermolaev, Y. Yu, J. Magn. Reson. 138 (1999) 28.
[15] E. Vinogradov, P.K. Madhu, S. Vega, Chem. Phys. Lett. 314 (1999) 443.
[16] U. Haeberlen, High Resolution NMR in Solids. Selective Averaging, Advances in Magnetic Resonance, vol. Suppl. 1, Academic Press, New York, USA, 1976.
[17] J.H. Shirley, Phys. Rev. 138 (1965) B979.
[18] D. Sakellariou, A. Lesage, P. Hodgkinson, L. Emsley, Chem. Phys. Lett. 319 (2000) 253.
[19] A. Lesage, D. Sakellariou, S. Hediger, B. Eléna, P. Charmont, S. Steuernagel, L. Emsley, J. Magn. Reson. 163 (2003) 105.
[20] B. Elena, G. de Paëpe, L. Emsley, Chem. Phys. Lett. 398 (2004) 532.
[21] M. Leskes, S. Steuernagel, D. Schneider, P. Madhu, S. Vega, Chem. Phys. Lett. 466 (2008) 95.
[22] S. Paul et al., J. Magn. Reson. 197 (2009) 14.
[23] E. Salager, R.S. Stein, S. Steuernagel, A. Lesage, B. Elena, L. Emsley, Chem. Phys. Lett. 469 (2009) 336.
[24] L. Mafra, R. Siegel, C. Fernandez, D. Schneider, F. Aussenac, J. Rocha, J. Magn. Reson. 199 (2009) 111.
[25] E. Vinogradov, P.K. Madhu, S. Vega, Chem. Phys. Lett. 354 (2002) 193.
[26] Y. Ishii, R. Tycko, J. Magn. Reson. 142 (2000) 199.
[27] I. Schnell, B. Langer, S.H.M. Söntjens, M.H.P. van Genderen, R.P. Sijbesma, H.W. Spiess, J. Magn. Reson. 150 (2001) 57.
[28] G.R. Goward, I. Schnell, S.P. Brown, H.W. Spiess, H.-D. Kim, H. Ishida, Magn. Reson. Chem. 39 (2001) S5.
[29] I. Schnell, K. Saalwächter, J. Am. Chem. Soc. 124 (2002) 10938.
[30] J.W. Wiench, C.E. Bronnimann, V.S.-Y. Lin, M. Pruski, J. Am. Chem. Soc. 129 (2007) 12076.
[31] K. Mao, J.W. Wiench, V.S.-Y. Lin, M. Pruski, J. Magn. Reson. 196 (2009) 92.
[32] D.H. Zhou, G. Shah, M. Cormos, C. Mullen, D. Sandoz, C.M. Rienstra, J. Am. Chem. Soc. 129 (2007) 11791.
[33] D.H. Zhou, C.M. Rienstra, Angew. Chem. Int. Ed. 47 (2008) 7328.
[34] D.H. Zhou, G. Shah, C. Mullen, D. Sandoz, C.M. Rienstra, Angew. Chem. Int. Ed. 48 (2009) 1253.
[35] F. Engelke, Concepts Magn. Reson. B 15 (2002) 129.
[36] S. Hediger, B.H. Meier, R.R. Ernst, Chem. Phys. Lett. 240 (1995) 449.
[37] G. Metz, X. Wu, S.O. Smith, J. Magn. Reson. A 110 (1994) 219.
[38] A. Ramamoorthy, C.H. Wu, S.J. Opella, J. Magn. Reson. 140 (1999) 131.
[39] B.-J. van Rossum, C.P. de Groot, V. Ladizhansky, S. Vega, H.J.M. de Groot, J. Am. Chem. Soc. 122 (2000) 3465.
[40] P. Tekely, P. Palmas, D. Canet, J. Magn. Reson. A 107 (1994) 129.
[41] A. Detken, E.H. Hardy, M. Ernst, B.H. Meier, Chem. Phys. Lett. 356 (2002) 298.
[42] P. Giannozzi et al., J. Phys.: Condens. Matter 21 (2009) 395502.
[43] M.A. Mehta, M.T. Eddy, S.A. McNeill, F.D. Mills, J.R. Long, J. Am. Chem. Soc. 130 (2008) 2202.
[44] S. Luca, D.V. Filippov, J.H. van Boom, H. Oschkinat, H.J.M. de Groot, M. Baldus, J. Biomol. NMR 20 (2001) 325.
[45] Z. Gan, J. Am. Chem. Soc. 128 (2006) 6040.
[46] A.J. Vega, J. Magn. Reson. 170 (2004) 22.
[47] S. Cavadini, S. Antonijevic, A. Lupulescu, G. Bodenhausen, J. Magn. Reson. 182 (2006) 168.
[48] Z. Gan, J.P. Amoureux, J. Trébosc, Chem. Phys. Lett. 435 (2007) 163.